NORSAR

ROYAL NORWEGIAN COUNCIL FOR SCIENTIFIC AND INDUSTRIAL RESEARCH

Scientific Report No. 2-84/85

SEMIANNUAL TECHNICAL SUMMARY

1 October 1984 – 31 March 1985

L. B. Loughran (Ed.)

Kjeller, July 1985

VII.2 Preliminary evaluation of the event detection and location capability of the small-aperture NORESS array

The new NORESS array in Norway has been operation since October 1984. The geometry of the array is shown in Fig. VII.2.1. The array has 25 short period vertical seismometers, arranged on concentric rings around the central site. Four of the 25 sites are occupied by three-component seismometers.

A data base of local and regional events has been collected, with the purpose of evaluating the event detection and location capability of the new array. As a first approach, we have concentrated our efforts on the study of a data set of 18 seismic events that occurred in the Baltic and Leningrad regions of the U.S.S.R. during the time period January-March 1985. The events are associated with mining activity and are all reported and located by the Finnish network of seismic stations. An example of one such event is shown in Fig. VII.2.2. Three distinct phases P, Sn and Lg can be seen for all 18 events. Spectra for noise preceding the P onset, the P phase, the Sn phase and the Lg phase are plotted together in Fig. VII.2.3 for one of the events. As can be seen, the P phase is very rich in high frequencies, while Sn and Lg approach the noise level from about 8 Hz. Note also the noise peak at around 6 Hz, which is typical of daytime noise samples.

Now, to assess the detection capability of the array, we have estimated the SNR gain by beamforming for the three phases P, Sn and Lg. This has been done by computing the signal loss and noise suppression and taking the ratio. The signal loss is the spectrum of the beam (with appropriate bearing and velocity depending on the phase type) divided by the average spectrum of all individual channels. Similarly, the noise suppression is the ratio of the spectrum of the noise beam (noise preceding the signal, shifted in the same way as the signal itself for the beamforming) to the average spectrum of all individual channels.

The noise spectra have been estimated using the indirect covariance method. We first estimate the correlation function by splitting a long data record into many windows, calculating a sample correlation function for each window, then averaging the sample correlation functions. Typically, we use 20 windows, each of which is 5 seconds long. Because the earth noise has such a large dynamic range, we prewhiten it prior to estimating the correlation function with a low-order prediction-error filter. The spectrum is then estimated by windowing the correlation function with a 3 second Hamming window, then computing the Fourier Transform. The spectral estimate obtained this way is compensated then for the effects of prewhitening.

The signal spectrum is calculated by windowing the signal with a 10% cosine taper window, 5 seconds long, then calculating the Fourier Transform and finally squaring the transform.

When we do direct comparison of the noise spectrum, which is a power density spectrum, with the signal, which is an energy density spectrum, we divide the signal spectrum by the length of the signal analysis window to convert energy density to power density. The two spectral quantities are then directly comparable. This has been done in Fig. VII.2.3.

The signal loss, noise suppression and SNR gain by beamforming have been computed for four different array configurations:

- All elements included ("ALLV" in the figures)
- All elements minus A-ring ("INTERMEDIATE")
- Center instrument, C-ring and D-ring ("TELEV")
- All elements minus D-ring ("HIFREQ").

In Fig. VII.2.4, noise suppression curves, representing averaging over the 18 events, are shown for all four array geometries. The horizontal lines represent $\sqrt{N}$ suppression of noise, where N is the number of sensors in the geometry under consideration. This is the expected level

for noise that is uncorrelated over the entire array. As can be seen, the "TELEV"-geometry is remarkably good in suppressing the noise in the 1.5-3.5 Hz band, while the other geometries approach the $\sqrt{N}$ level for various frequencies, but do not show better noise suppression than $\sqrt{N}$. These results partly reflect on the SNR gains shown in Fig. VII.2.5. the signal losses (not shown) tend to be larger for the larger geometries (including outer rings) because of the decaying signal correlation with increasing station separation. The overall effect is to level the gain curves, and we can see from Fig. VII.2.5 that only at fairly low and fairly high frequencies do the gain curves for the different geometries deviate substantially.

For the Sn and Lg phases, the "noise suppression" estimates reflect suppression by beamforming of the P and Sn coda, respectively, i.e., we address the problem of detecting a secondary phase in the coda of a preceding phase. Results shown in Fig. VII.2.6 are for the Lg phase and correspond to the best SNR result obtained among the four geometries. SNR-gain is now well below $\sqrt{N}$, essentially because of failure to suppress the Sn coda, which propagates with similar phase velocity and azimuth as the Lg onset. Still, there is a 6 dB gain from beamforming at 1.2 Hz.

Fig. VII.2.7 shows the P onset for a Novaya Zemlja explosion (distance approx. 20^{o}) recorded on NORESS, and the SNR gain by beamforming computed as before for the "TELEV" configuration. In the frequency range 1.0-2.7 Hz the gain is better than $\sqrt{N}$, because of a very modest signal loss in combination with optimum noise rejection, as for the "TELEV"-configuration in Fig. VII.2.3. The same result is visualized in the time domain in Fig. VII.2.8.

Our approach to the location performance evaluation has been to compute narrow-band FK-spectra for the P, Sn and Lg signals for the events in the data base. FK-spectra have been computed for the array subsets given above and for frequencies corresponding to distinct spectral maxima for each phase. Typical results are given in

Table VII.2.1 for one event. As can be seen, the analysis frequency is the critical parameter, and more so than the array subgeometry used in the evaluation of the FK-spectra. According to these results, then, the arrival azimuth varies fairly strongly with frequency and due care must be taken in selecting the analysis frequency. To gain more insight into these frequency-dependent lateral refraction effects, we have computed the broad-band maximum likelihood FK-spectra for a number of phases. One example is shown in Fig. VII.2.9, where the azimuth's dependency on frequency is given implicitly in the contour plot. The azimuth value of 89.5 serves to illustrate that the broad-band FK tends to give more stable estimates than those derived from narrow-band FK-spectra.

The research effort continues with analysis of events from other regions, in order to obtain the capabilities of the new NORESS array for local and regional events from all source regions of interest. As experience is gained, the results from this study will be utilized directly in the online processing of NORESS data.

S. Mykkeltveit
D.B. Harris, Lawrence
Livermore National Laboratory
T. Kværna

	P at 3.40 Hz		P at 6.35 Hz		Sn at 2.20 Hz		Lg at 1.33 Hz		Lg at 1.80 Hz	
Array	Vel	Az	Vel	Az	Vel	Az	Vel	Az	Vel	Az
HIFREQ	11.71	80.8	9.73	92.3	5.05	86.1	4.55	95.5	4.31	109.0
ALLV	11.58	86.1	10.14	95.8	5.02	84.0	4.29	95.4	4.07	106.9
INTERM	11.52	86.2	10.15	95.9	5.02	84.0	4.29	95.5	4.08	105.7
TELEV	11.51	86.3	10.07	98.1	5.03	84.0	4.28	95.0	4.10	102.3

Table VII.2.1 Narrow-band FK-results for one event in the Baltic-Leningrad region data base. According to the location reported by the network of Finnish seismic stations, the true azimuth for NORESS is 91.6°.

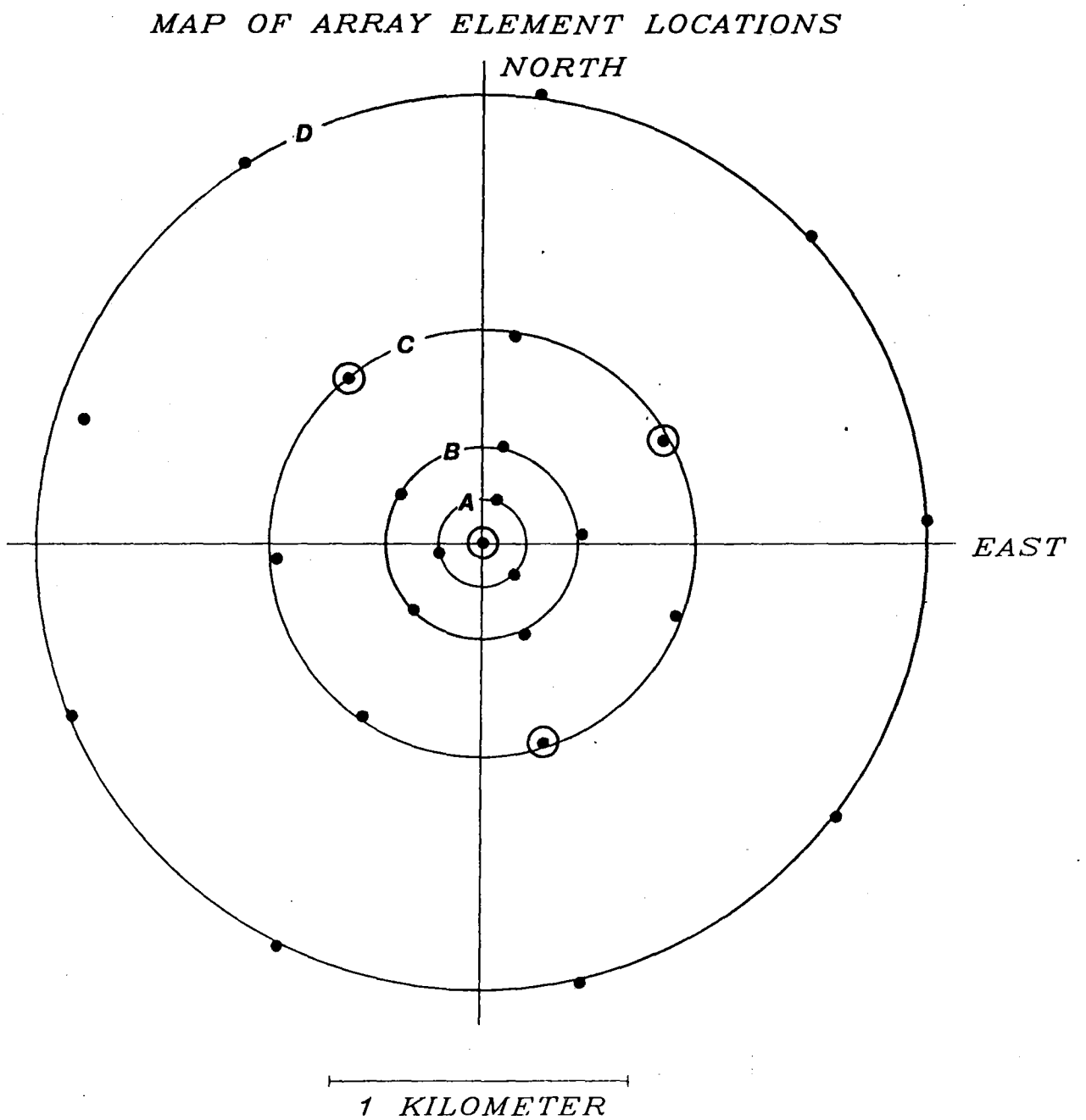

Fig. VII.2.1 Geometry of the new NORESS array. The four three-component stations are marked with special symbols.

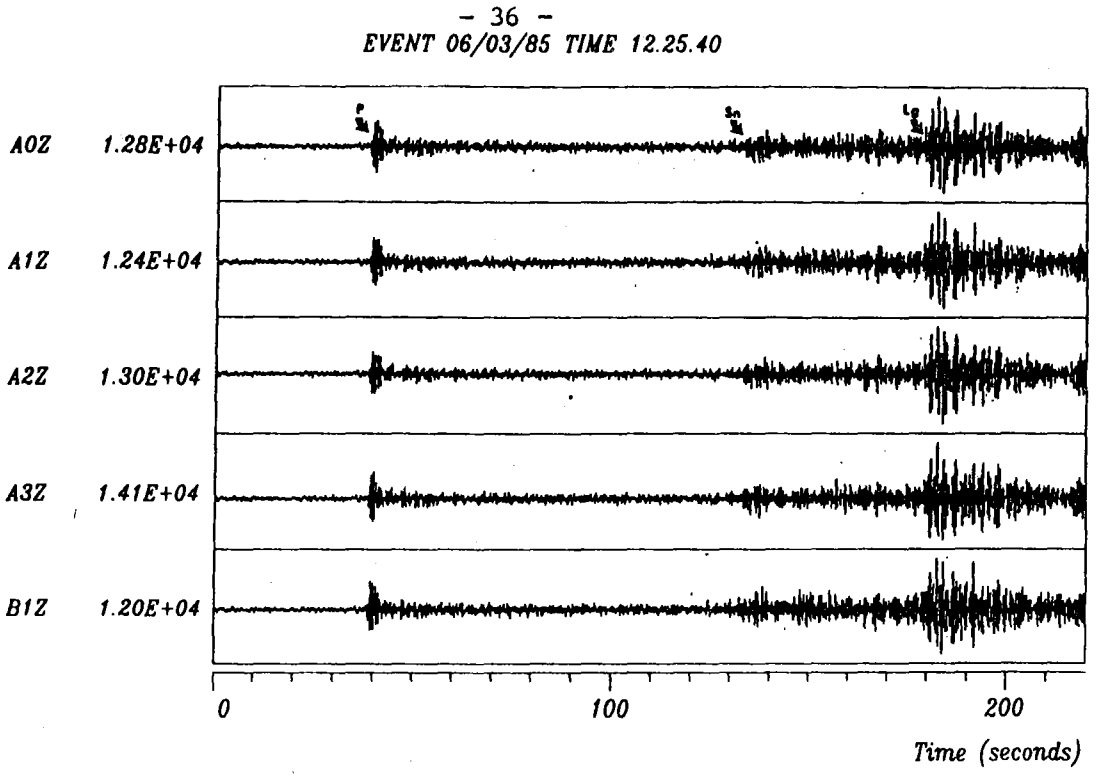

Fig. VII.2.2 Example of event from the Leningrad region, with P, Sn and Lg phases.

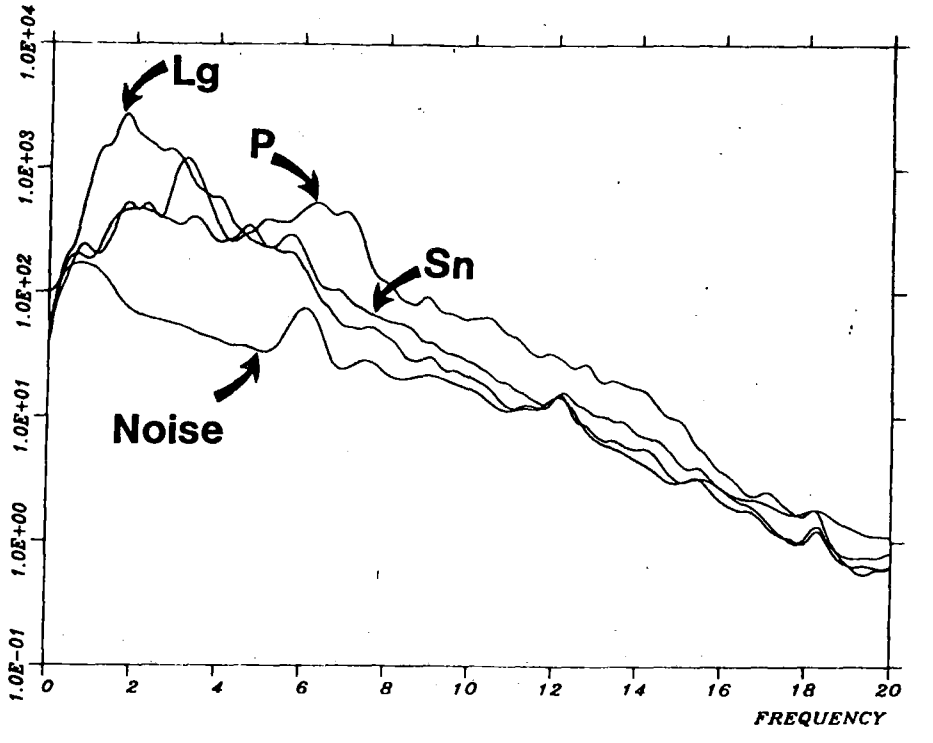

Fig. VII.2.3 Spectra for the P, Sn and Lg in Fig. VII.2.2 and for noise preceding the P arrival.

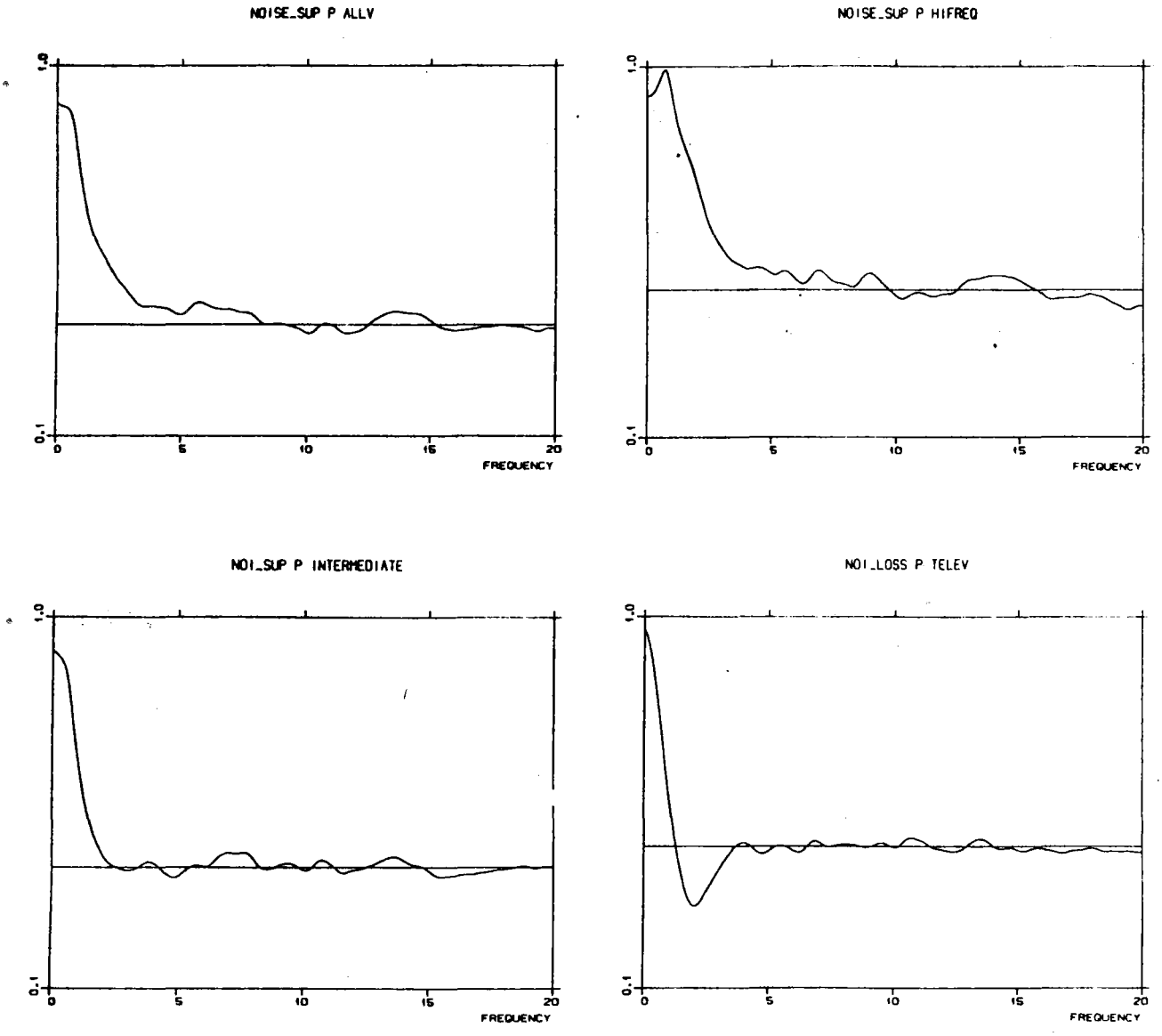

Fig. VII.2.4 Noise suppression for the four array subgeometries. The horizontal line represents $\sqrt{N}$ noise rejection, where N is the number of sensors in each subgeometry. The vertical scale is logarithmic.

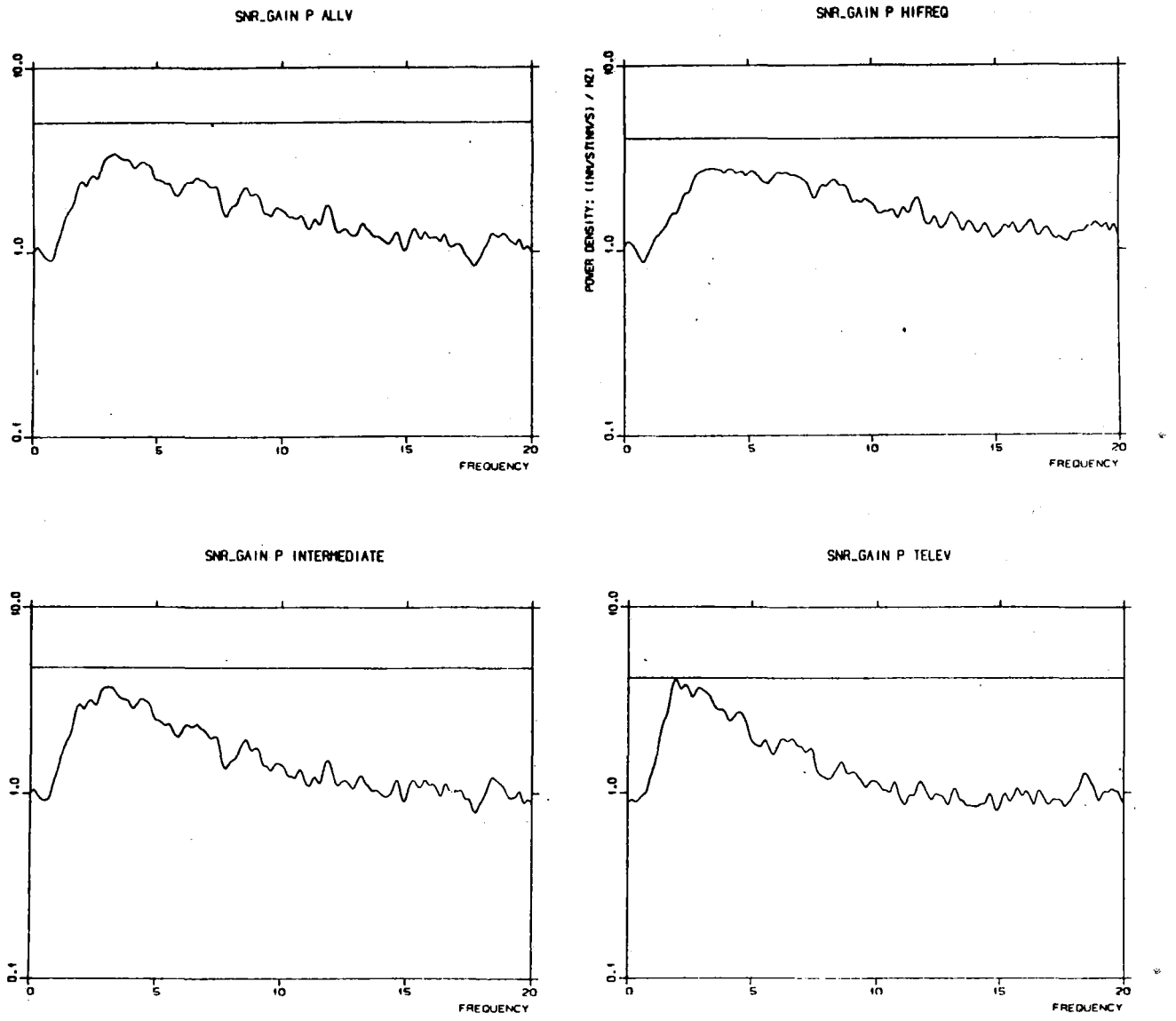

Fig. VII.2.5 SNR gain by beamforming of regional P phase for the four array subgeometries. The horizontal line represents $\sqrt{N}$ gain, where N is the number of sensors in each subgeometry. The vertical scale is logarithmic.

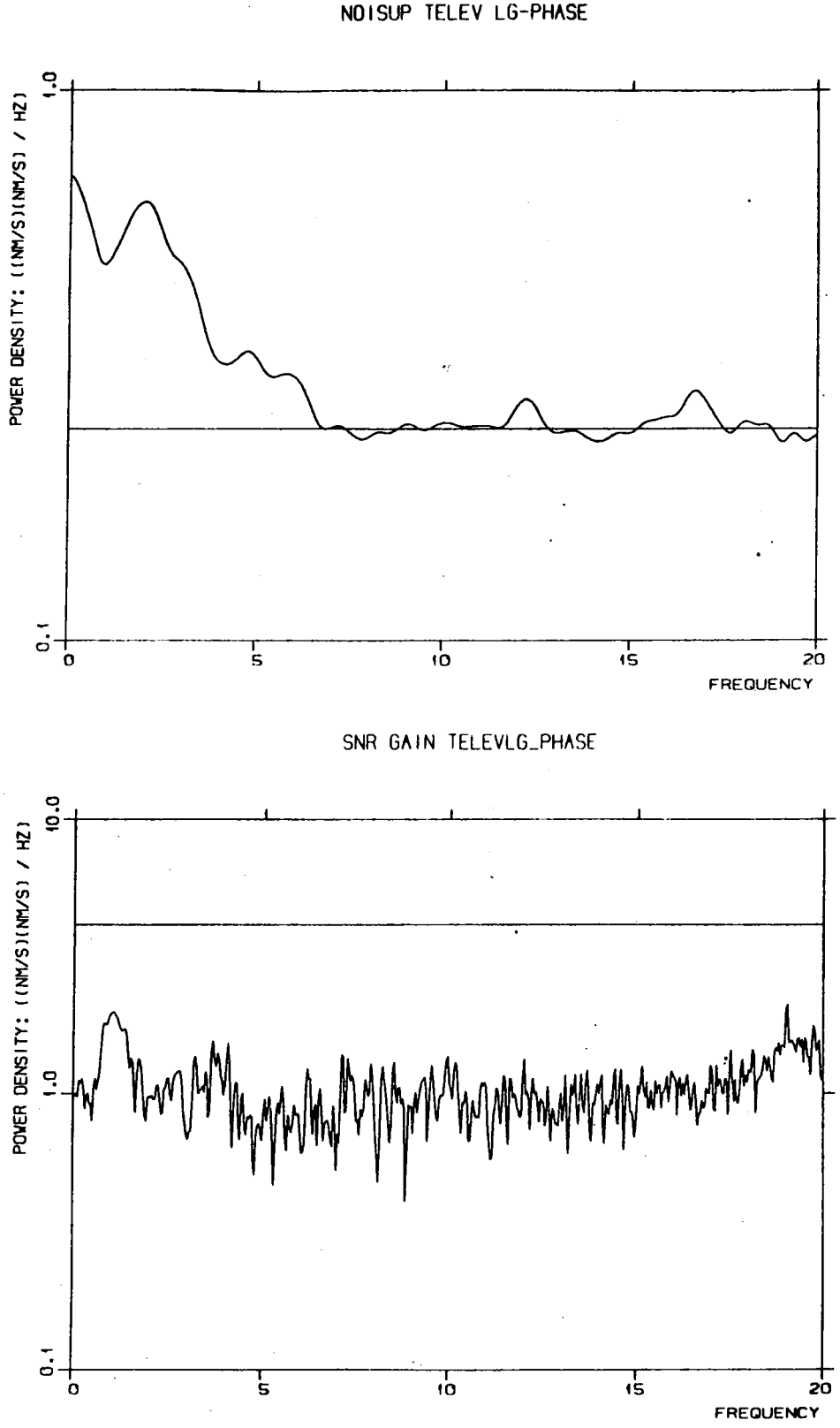

Fig. VII.2.6 Noise suppression and SNR gain for the Lg phase for subgeometry "TELEV". Horizontal lines represent $\sqrt{N}$-noise rejection (upper plot) and $\sqrt{N}$-beamforming gain (lower plot), with N = 17 for this subgeometry. Vertical scales are logarithmic.

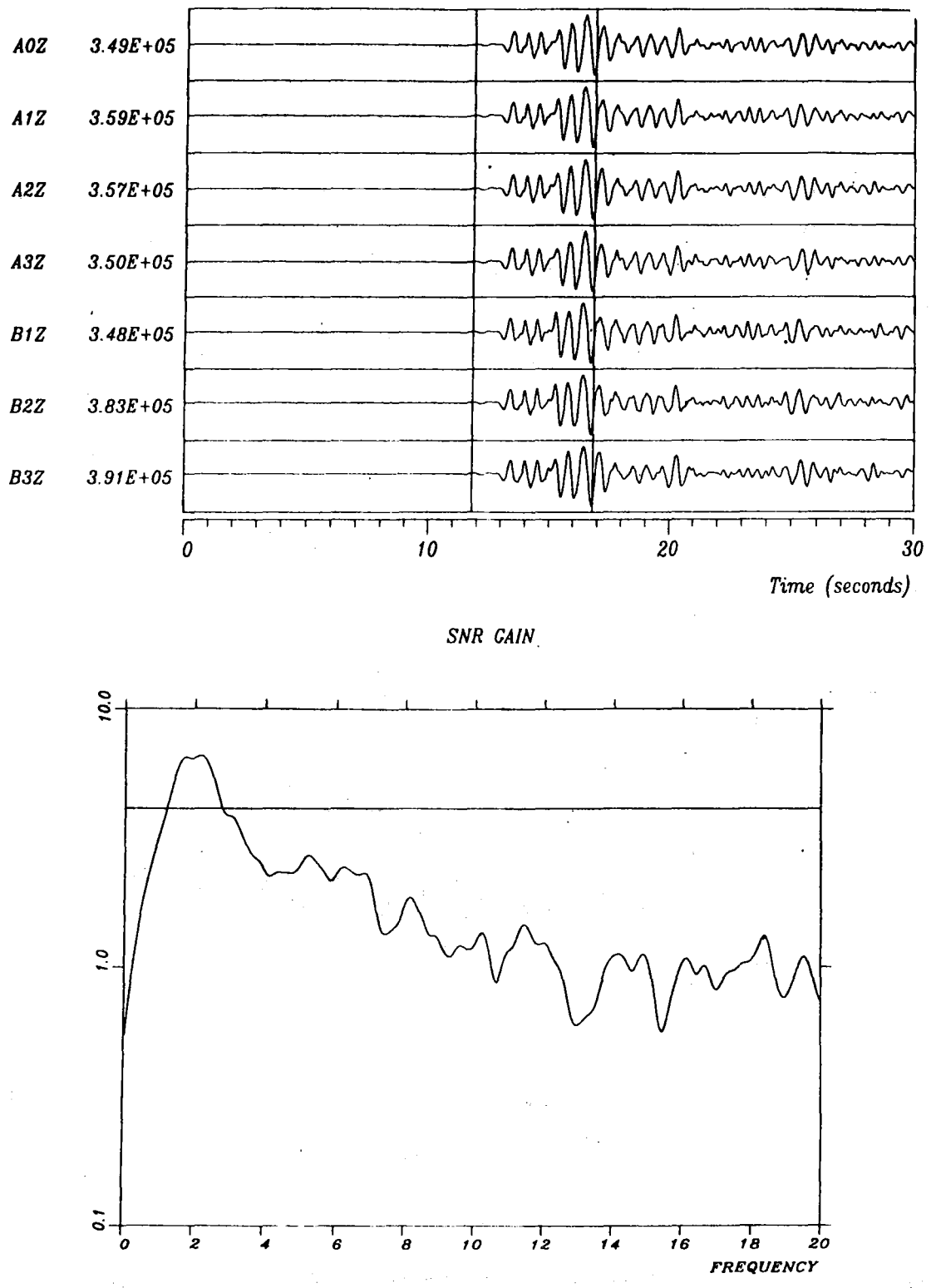

Fig. VII.2.7 Beamforming gain for array "TELEV" for P-arrival from Novaja Zemlja event. P-wave data analysis window on top. The horizontal line in the gain plot indicates $\sqrt{N}$ gain, with N = 17 for this subgeometry.

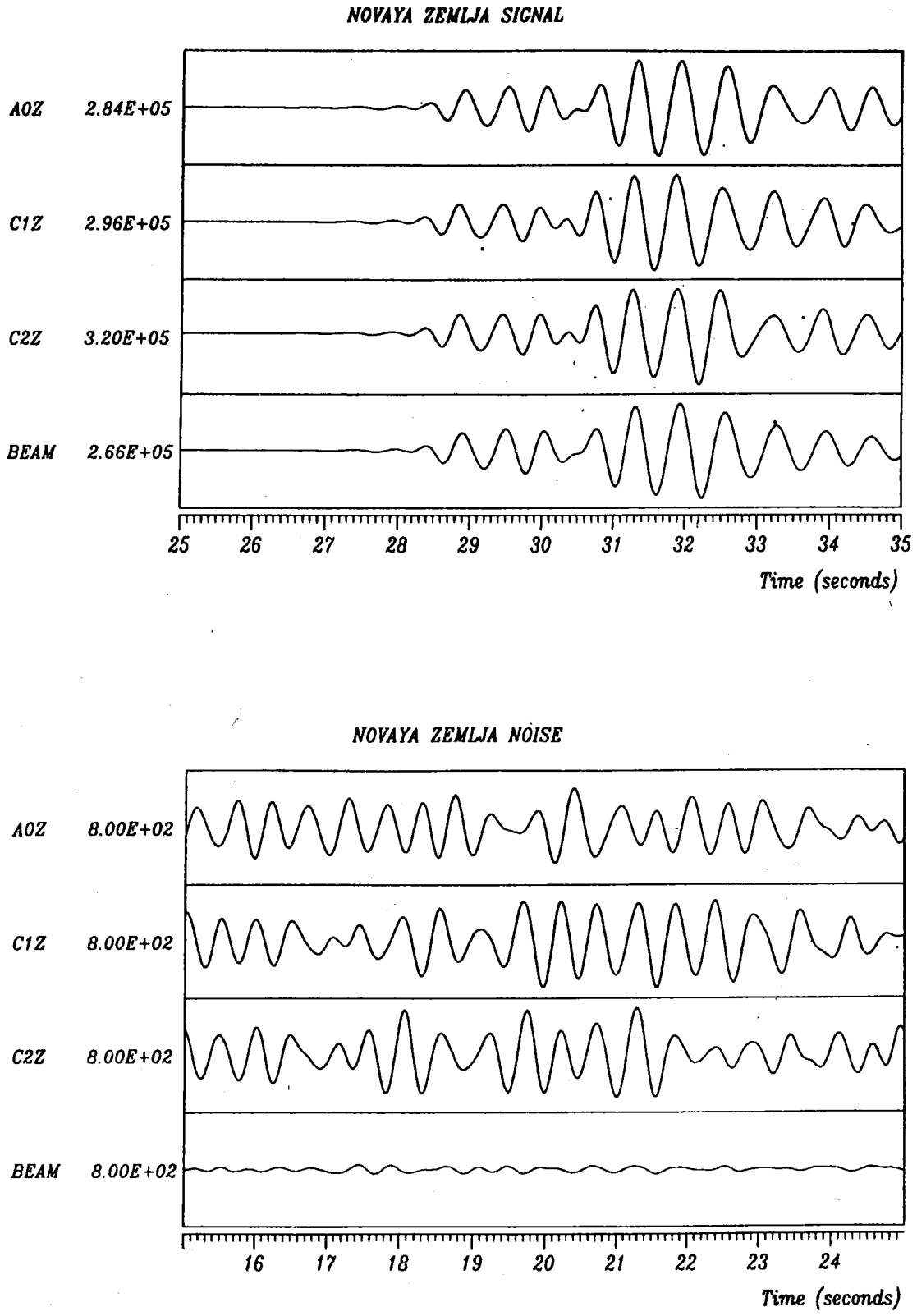

Fig. VII.2.8 Time domain illustration of the SNR-gain results in Fig. VII.2.7. Top: Normalized plot of three single channels (out of the 17 participating in the beam) and the beam, showing a very modest signal loss. Bottom: Noise rejection obtained on preceding noise (true amplitude plot). The filter bandpass is 1.3-2.5 Hz, corresponding to the peak in the gain curve in Fig. VII.2.7.

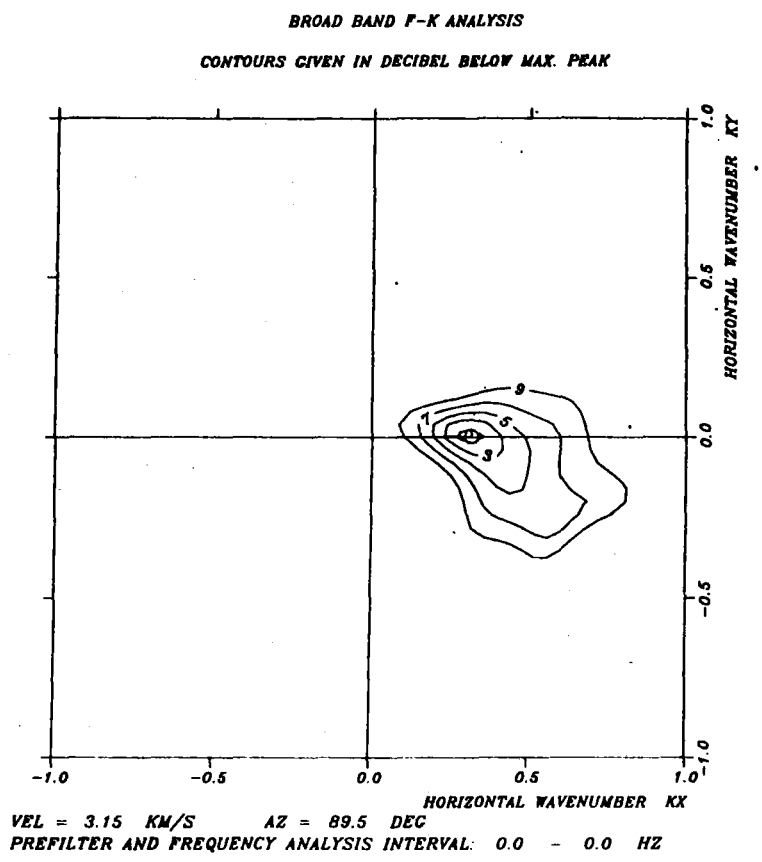

Fig. VII.2.9 Broad-band FK-analysis for the Lg phase of the event used in Table VII.2.1. In order to obtain the velocity corresponding to the peak, the value of 3.15 km/s must be multiplied by the dominant frequency of the Lg signal (1.33 Hz) to yield a phase velocity of 4.19 km/s.